Thermal degradation of solid porous materials exposed to fire.

K.-T Nguyen, B. Batiot, V.V. Mourzenko, T. Rogaume, J.-F. Thovert

. Institut PPRIME - CNRS, SP2MI, BP 30179, 86960 Futuroscope Chasseneuil Cedex

Abstract :

Thermal degradation of solid materials, an important source of gaseous combustible matter during fire events, is addressed by numerical simulations. Based on intrinsic data including a chemical model obtained by measurements on samples small enough to prevent any limiting influence of heat and mass transports, simulations are conducted on a larger scale by taking into account the coupling between the chemical reactions and the various transport mechanisms. Thus, the response of the material undergoing any scenario of ambient conditions can be determined. These simulations are performed on the Darcy scale in the prescribed scenarios of standardized tests, in order to establish a typology of behaviors and to identify the key processes and governing parameters. Later, they could be directly coupled with a fire simulation tool on the global scale, accounting for the influence of the emitted species on the fire development.

Résumé :

La dégradation thermique de matériaux solides, importante source de gaz combustibles qui contribuent à nourrir le feu, est abordée par simulations numériques. Sur la base d'un modèle chimique intrinsèque, issu de mesures à échelle assez petite pour éliminer l'influence limitante de processus de transport, des simulations sont conduites à plus grande échelle, afin de prendre en compte les couplages entre réactions et mécanismes de transport et de prédire la réponse du matériau soumis à un scénario quelconque de conditions ambiantes. La description se situe à l'échelle de Darcy. Elle vise d'abord à établir une typologie de comportements, à identifier les processus et paramètres clés. Par la suite, un couplage pourra être établi avec un code de simulation du feu à l'échelle globale, qui pourra alors prendre en compte l'influence des espèces émises sur le développement du feu.

Mots clefs : **Porous media ; Pyrolysis ; Combustion**

1 Introduction

Combustion of porous solids involves a first step of thermal degradation with emission of volatile species, followed by the combustion of the gaseous species in the surrounding space. Hence, thermal degradation is a process of crucial importance since the combustible gaseous species released by the pyrolysis greatly contribute to feed the fire which causes it.

The simulation of the process on the global scale (fire accident on the building scale, plant, forest, ... or operation of a reactor) requires a good description of this first step as a function of the ambient parameters such as temperature and oxygen concentration. But characterizations of thermal decomposition by small or large scale measurements often yield different responses, because of the coupling in the latter case between the chemical reactions and the various heat and mass transport processes. The purpose of this work is to make the connection between these two points of view, and to predict the macroscopic behavior as a function of the constituent properties, of the microstructural characteristics and of the ambient conditions. Thus, expensive large scale physical tests to be repeated for any specific scenario under consideration could be replaced by numerical simulations based on intrinsic data which can be obtained at a much lesser cost.

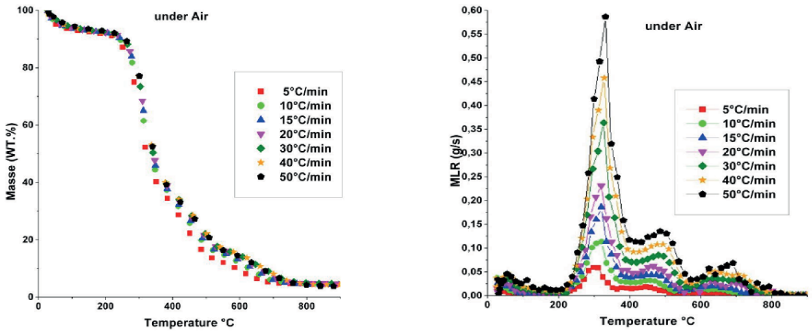

FIGURE 1 – Sample mass (left) and mass loss rate (right) as functions of temperature in TGA experiments under air with various values of the temperature increase rate.

This requires a detailed account of the chemical and thermomechanical mecanisms, and of their coupling on various scales. A description of the chemical processes, including a reaction scheme and the associated thermokinetic parameters can be obtained by thermogravimetric measurements on samples small enough to prevent any limiting influence of the heat and mass transports [1]. Numerical simulations can then be conducted on a larger scale, to determine the response of the material in a given geometrical configuration, undergoing any scenario of ambient conditions.

In a first step, these simulations are performed on the Darcy scale and in prescribed scenarios which correspond to standardized physical tests. This will allow to establish a typology of behaviors, to identify the key processes and their governing parameters, and to validate the numerical predictions. In a later stage, microscopic investigations could be conducted for a better characterization of some processes and for the determination of relevant effective coefficients. Ultimately, this description of the material degradation could be directly coupled with a simulation tool of the fire on the global scale, which would provide the time dependent ambient conditions, and would take the influence on the development of the fire of the emitted species into account.

2 Chemical model

A commercial plywood was characterized by TGA/DSC (see Fig. 1) and a simplified chemical model was deduced [2]. A simpler material (solid pine wood) is currently being investigated, with a better characterization of the emitted species. These data will be used as soon as available. Meanwhile, the simulations are run with the plywood data. The reaction scheme involves three main steps, drying, pyrolysis and combustion, which can be decomposed in several sequential reactions. Each reaction consumes a solid species, produces a new one and releases gases. For a simpler presentation, the four steps of pyrolysis are lumped here into a single pyrolytic reaction, and the two oxidative reactions into a single one. Note however that this simplification is only intended for the readability of the results. It does not significantly ease the calculations. The same physical features take place than with the full chemical model, with the same sudden changes of regime and overall gas emission. Hence, the reaction scheme is summarized as

$$S_1 \rightarrow \nu_1\, S_2 + (1-\nu_1)\, g_1 \tag{1}$$
$$S_2 \rightarrow \nu_2\, S_3 + (1-\nu_2)\, g_2 \tag{2}$$
$$S_3 + \nu_O\, O_2 \rightarrow \nu_3\, S_4 + (1+\nu_O-\nu_3)\, g_3 \tag{3}$$

S_i denotes the successive states of the solid material, namely wet wood (S_1), dry wood (S_2), char (S_3) and residual ashes (S_4). The ν's are mass stoichiometric coefficients. The reaction kinetics are described by Arrhenius law. For instance, the comsumption rate of solid i in reaction (i) and its production rate in reaction $(i-1)$ are given by

$$C_{s_i}^{r_i} = \rho_{s_i}\, \rho_{O_2}^{b_{r_i}}\, A_{r_i}\, e^{-\frac{E_{r_i}}{RT}} \qquad (\text{with } b_{r_i} = 0 \text{ or } 1) \tag{4}$$
$$P_{s_i}^{r_{i-1}} = \nu_{i-1}\, C_{s_{i-1}}^{r_{i-1}} \tag{5}$$

S_i denotes the successive states of the solid material, *e.g.*, char (S_6) or residual ashes (S_8).

3 Thermomechanical model

We describe the processes which take place within the solid exposed to thermal aggression. It is assumed that ambient conditions do not significantly vary along its surface, on a scale of the order of the thickness. Therefore, the problem is treated as one dimensional. The origin of the x-axis is set at the solid surface. Of course, the outer conditions may vary on a larger scale, either along a same wall or on different walls exposed to the fire. The response of the material will vary accordingly, and can be predicted by the present tool at any location deemed necessary for the global fire event simulation. However, two- or three-dimensional features such as significant transverse heat or mass transfers due for instance to end-effects are not accounted for at this stage.

The main equations are the mass and energy balances. They include the various transport mechanisms, namely convection, species diffusion and heat conduction, and sink/sources terms resulting from the chemical reactions. The momemtum equation is embodied in Darcy's law. Mass conservation for the condensed and gaseous species imply that

$$\frac{\partial \rho_{s_i}}{\partial t} = \sum_j \left(P_{s_i}^{r_j} - C_{s_i}^{r_j}\right) \tag{6}$$

$$\frac{\partial}{\partial t}\left(\varepsilon \rho_{g_i}^*\right) + \frac{\partial}{\partial x}\left(\rho_{g_i}^* \ \overline{v_g}\right) - \frac{\partial}{\partial x}\left(\overline{D} \ \rho_g^* \ D_{g_i} \ \frac{\partial Y_{g_i}}{\partial x}\right) = \sum_j \left(P_{g_i}^{r_j} - C_{g_i}^{r_j}\right) \tag{7}$$

Summations for the source/sink terms run over all the reactions where the species is involved. ρ_X denotes a bulk density (mass of X per volume of porous material), and ρ_X^* a phase density (mass per volume occupied by species X). For instance, for gaseous species, $\rho_{g_i} = \epsilon \rho_{g_i}^*$, where ϵ is the porosity. Y_{g_i} and D_{g_i} are the mass-fraction of species g_i in the gas and its molecular diffusion coefficient. $\overline{D}$ is the diffusivity coefficient of the porous medium. $\overline{v_g}$ is the barycentric filtration velocity of the gas mixture, related to the pressure gradient by Darcy's law

$$\overline{v_g} = -\frac{K}{\mu}\frac{\partial P}{\partial x} \tag{8}$$

where P is the pressure, μ the dynamic viscosity and K the permeability. Local thermal equilibrium is assumed, *i.e.*, the same temperature T is assumed to prevail in the solid and gaseous phases at any position x. Therefore, the energy conservation equation reads

$$\frac{\partial}{\partial t}\left[\left(\sum_i \phi_i \ \rho_i^* \ C_{pi}\right) T\right] + \frac{\partial}{\partial x}\left(\rho_g^* \ \overline{v_g} \ C_{pg} \ T\right) - \frac{\partial}{\partial x}\left(\overline{\lambda} \ \frac{\partial T}{\partial x}\right) = \sum_j \left(\Delta H^{r_j} \ C_{s_j}^{r_j}\right) \tag{9}$$

where the first summation runs over all chemical species i, with heat capacity C_{pi}, occupying a volume fraction ϕ_i. $\overline{\lambda}$ is the macroscopic thermal conductivity of the porous medium. The last summation runs over all the chemical reactions j, with mass enthalpy ΔH^{r_j}.

The balance equations have to be supplemented with constitutive equations. The state equation of perfect gases is applied in the pores, the molecular diffusion coefficients D_{g_i} are evaluated by Chapman-Enskog's formula with Lennard-Jones' parameters [3], by regarding g_i as a dilute species in air, and the variations of viscosity with temperature are described by Sutherland's formula. In addition, effective properties of the porous medium have to be provided. In the forthcoming example, porosity is deduced from the bulk density of the condensed phases, permeability is assumed to vary according to a cubic law of porosity, $\overline{D}$ is taken equal to the porosity, and a volumetric mixing rule is applied to evaluate the mean thermal conductivity $\overline{\lambda}$. A radiative contribution is added to $\overline{\lambda}$, designed to make the volume elements where only a small amount of ashes is left nearly transparent to radiative exchanges with the exterior space. Its contribution is negligible in other situations.

Finally, boundary conditions have to be specified. The backside $x = L$ is assumed to be impermeable and adiabatic. Other conditions could of course be easily substituted. On the exposed face $x = 0$, an

incident radiative heat flux is specified, and a flux σT^4 is emitted, *i.e.*, unit emissivity (and adsorptivity) is assumed which is an approximation. It has been shown in [4] that it varies both with the wavelength and the degree of degradation. These variations can be accounted for if the spectral characteristics of the incident flux are known. Atmospheric pressure is imposed and diffusive/conductive species and heat exchanges with the outside are proportional to the differences of concentration or temperature with prescribed ambient conditions which prevail at some distance from the surface.

4 Numerical implementation

The problem is discretized in space in a second order finite volume formulation. An upwind scheme is applied for the convective terms. The main difficulty of the simulations rests with the management of the time stepping. A first version was implemented with an explicit first order time discretization. An adaptative time step is imperative because of the strong non linearities in the problem which give rise to abrupt changes of regime. Sudden onsets of chemical reactions can occur, when temperature reaches required values, because of the exponential form of Arrhenius law. In turn, this can cause the sudden release of a large amount of gases, with strong impact on the mixture composition (from which pressure is deduced), and on the convective contribution to the transports. The time step δ_t is governed by various criteria which restrict the variations of the parameters. In addition, stability criteria must be satisfied in an explicit scheme and those associated with the diffusive processes (species diffusion, heat conduction and especially Darcy's law) result in very small time step values.

A time implicit version is currently being developed. Since most of the coefficients in the balance equations (6-9) depend on the current state, and in many cases non-linearly (*e.g.*, the reaction rate given by Arrhenius law, the radiative emission at the exposed surface, or the pressure response to changes in the gas mixture composition), a Picard iteration scheme is used. An implicit set of linear equations for the variations of the variables ρ_{g_i}, ρ_{g_i} and T during a time step is written first with the current values of the coefficients in (6-9). It is solved, and the coefficients of (6-9) are re-evaluated by using these new data. This is repeated until convergence. This alleviates some of the limitations for the time step, but depending on the current state of the system δ_t can still need to be very small in order for the Picard loop to converge. An optimal management in this respect is a key issue for the performance and robustness of the simulator. In the following examples, the grid step is 600 μm and the adaptative time step varies in the range of 1 ms during quiescent periods to 0.1 ms during more active episodes.

5 Example of results

Results obtained with the latest (implicit) version in the reference situation of a standardized physical test are presented here. A 18 mm thick plywood sample is placed in a cone calorimeter. It is initially cold and submitted to a steady 40 kW/m^2 incident radiative flux. Ambient conditions on the exposed face are standard atmospheric pressure and oxygen concentration, while no-flux conditions are imposed on the opposite face.

The composition profiles in the material are shown in Fig.2 at successive times. In the initial state (a), dry wood and water are distinguished. At t=350 s (b), drying is almost complete. Only a small amount of water remains in the deepest region. The wood is intact at $x \geq$8 mm. The pyrolytic reaction takes place in the range x=3$\sim$8 mm, producing char. The oxidation of the char is already begun in the superficial region, leaving ashes. The pyrolysis and oxidation fronts are seen to progress in the later stages (c-e), until only ashes remain in the final stage (f).

Figure 3 shows the density, temperature and pressure profiles at the same instants. T rises very fast in the superficial region due to the radiative influx, and more progressively in the depth, because of the endothermal pyrolysis and of the strong convective heat transport toward the outside by the released gases. Later, the situation is reversed. The temperature profiles peak at the position of the exothermal oxidation front. Pressure is seen to significantly increase during the pyrolytic step, due to the massive gas emission. It returns to normal during the oxidation step, whose rate is limited by the diffusive oxygen supply and produces gas at a much smaller rate. The net fluxes of gaseous species through the

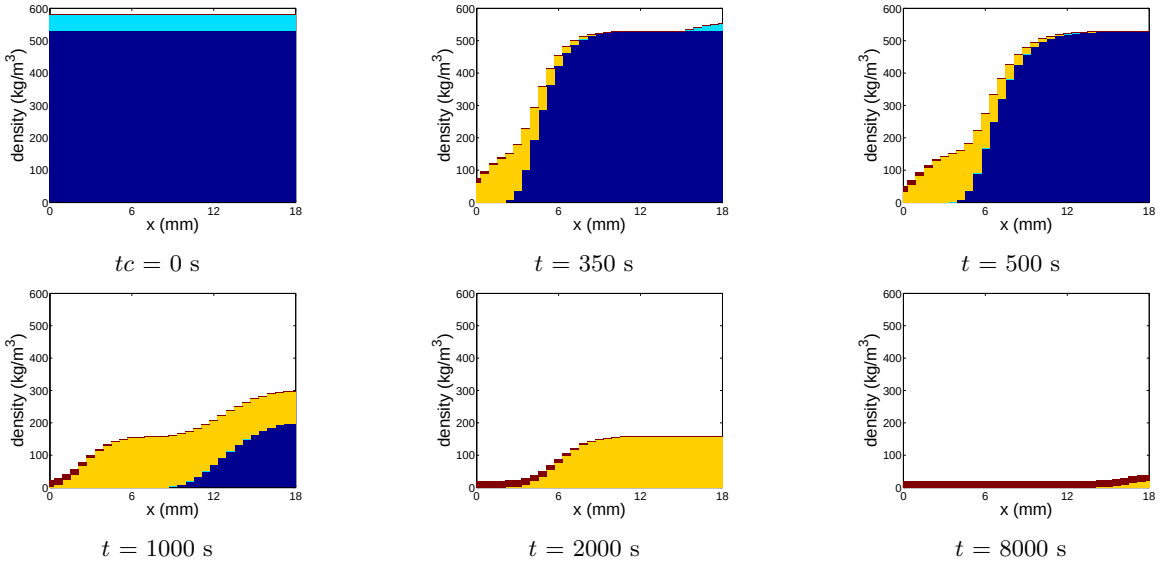

FIGURE 2 – Composition profiles at successive times. Colors correspond to water (cyan), dry wood (blue), char (orange), ashes (brown).

sample surface x=0 are shown in (d) as functions of time. Finally, the profiles of the reaction rates are shown in (e) at t=350 s (see Fig.2b). Although the chemical reactions occur mostly sequentially in TGA conditions, it is observed here that they can all take place simultaneously at various positions of a thick piece of material because temperature is not uniform. The evaporation front is at $x \approx$16 mm in Figs.2b and 3e. Water remains beyond this point, where temperature has not yet reached 100°C. A broad pyrolysis front exists at $x \approx$5 mm, and oxidation follows soon after.

Finally, Fig.4 compares the mass losses in the simulation and in the experiment. Temperature at various depths is plotted as a function of time in Figs.4b,c. The global trends are in agreement, although quantitative differences exist. This can easily be explained by uncertainties in the thermochemical data and in the effective transport coefficients. In addition, the temperature evolution on the backside suggests that the adiabatic condition is not realized in the experimental set-up. Improved simulations and a better agreement should be achievable when more reliable data are available.

6 Conclusion and perspectives

The results of the simulations are promising, with all the trends in good agreement with the experimental observations. Although some aspects of the physical model could be improved, for instance by a better description of the multiconstituent diffusion in the gas mixture, the critical issue for the accuracy of the prediction is currently the reliability of the input data and especially of the chemical model and associated thermokinetic parameters and of the values of the effective transport coefficients of the material in its initial and degraded states. Hence, the main part of the current effort is focused on the improvement of the efficiency, stability and robustness. These are difficult but essential objectives, in such problems where a great variety of non linear phenomena needs to be included, and which give inherently rise to violent transient episodes.

The other direction of development, for practical applications, is the coupling of this model with a global scale fire simulation tool. The stand-alone application presented here is a simple test case. Others are considered, with other scenarios for the incident radiative flux, and/or modified boundary conditions aiming to simulate the existence of a flame near the solid surface, where the pyrolytic gases burn, consuming oxygen and producing heat, part of which radiates back to the solid. However, the ultimate goal is to interface the small scale simulations within the wall material with a larger scale, global simulation of the fire event. The latter would provide the real history of ambient conditions for the solid degradation, and take its response into account in the prediction of subsequent developments.

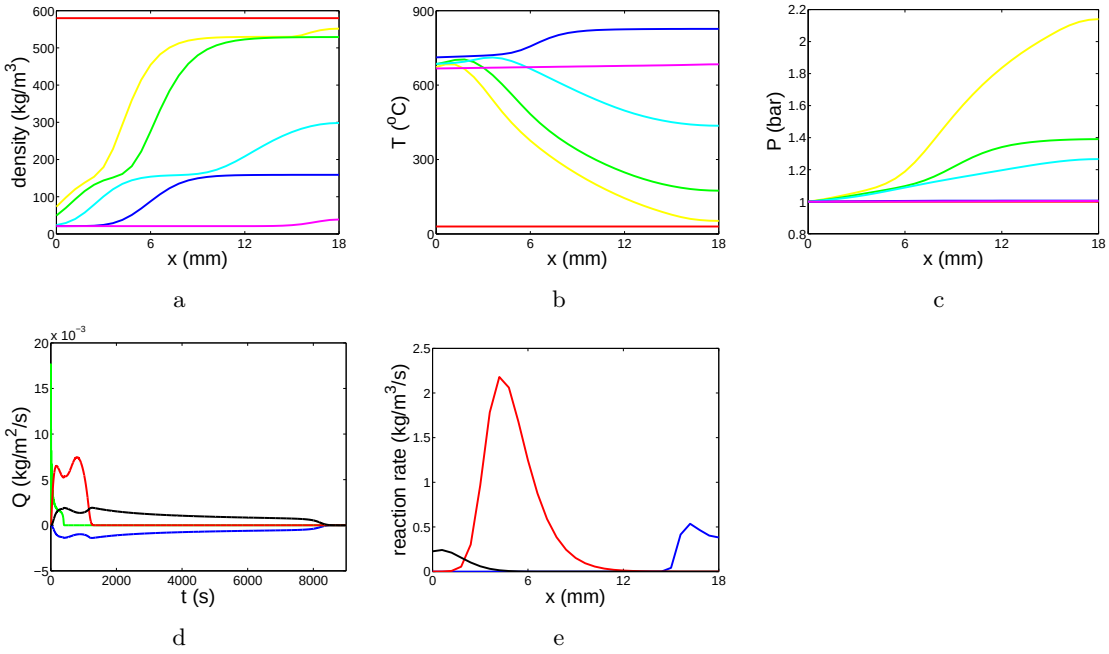

FIGURE 3 – Density profiles (a) at successive times t=0, 350, 500, 1000, 2000 and 8000 s, from top to bottom. Temperature (b) and pressure (c) profiles at the same instants. Gas emission/comsumption rates (d) as functions of times : water (green), products of pyrolysis (red) and combustion (black), oxygen (blue). Reaction rates at t=350 s (e) : evaporation (blue), pyrolysis (red), oxidation (black).

Références

[1] Bustamante Valencia L., T. Rogaume, E. Guillaume, G. Rein, J.L. Torero 2009 Analysis of principal gas products during combustion of polyether polyurethane foam at different irradiance levels. *Fire Safety Journal* **44** 933-940

[2] Fateh T. 2011 Etude expérimentale et numérique de la cinétique de dégradation thermique de contreplaqués en bois. Thèse de doctorat de l'ENSMA, Poitiers.

[3] Bird R.B., W.E. Stewart, E.N. Lightfoot 1960 *Transport phenomena*, Wiley, New York

[4] Boulet P., Parent G., Acem Z., Rogaume T., Fateh T., Zaida J. and Richard F. 2012 Characterization of the radiative exchanges when using a cone calorimeter for the study of the plywood pyrolysis, *Fire Safety Journal* **51** 53-60

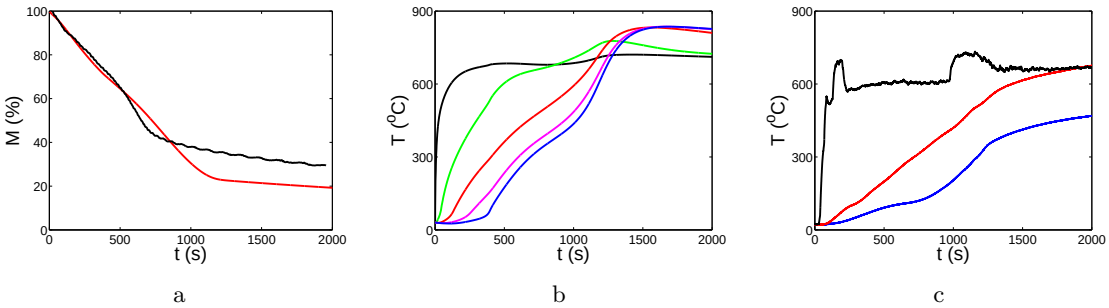

FIGURE 4 – Sample mass evolution along time (a) in the simulations (red) and in the experiment (black). Temperatures in the simulation (b) and in the experiment (c), at x=0 (black), 4.5 mm (green), 9 mm (red), 13.5 mm (magenta) and 18 mm (blue), as functions of time.